IEEE Access
Multidisciplinary | Rapid Review | Open Access Journal

Received January 21, 2020, accepted February 10, 2020, date of publication February 14, 2020, date of current version February 25, 2020.

Digital Object Identifier 10.1109/ACCESS.2020.2974007

Novel Evanescent-Mode Cavity Filter With Reconfigurable Rat-Race Coupler, Quadrature Coupler and Multi-Pole Filtering Functions

JUNCHEN LAI[1], TAO YANG[1], (Senior Member, IEEE), PEI-LING CHI[2], (Senior Member, IEEE), AND RUIMIN XU[1], (Member, IEEE)

[1]Department of Microwave Engineering, University of Electronic Science and Technology of China, Chengdu 611731, China
[2]Department of Electrical and Computer Engineering, National Chiao Tung University, Hsinchu 300, Taiwan

Corresponding author: Tao Yang (yangtao8314@uestc.edu.cn)

ABSTRACT A novel evanescent-mode cavity filter with multiple reconfigurable functions including filtering rat-race coupler, filtering quadrature coupler and multi-pole filtering is proposed in this paper. It simply consists of four substrate integrated waveguide (SIW) evanescent-mode cavity resonators which are arranged in a ring loop. By loading piezoelectric actuators on top of each resonator and inserting varactors between adjacent resonators, the structure can achieve multiple reconfigurable functions among filtering rat-race coupler, filtering quadrature coupler and single-ended multi-pole filters, in addition to continuously frequency, independent bandwidth, and power-division tuning. Measurement shows that the filtering quadrature coupler corves a frequency range of 2.08-3.00 GHz with insertion loss of 2.99 ± 0.31dB, while the filtering rat-race coupler corves a frequency range of 2.31-2.71 GHz with insertion loss of 2.97 ± 0.13dB; The single-ended filter can be switched among two-pole, three-pole, and four-pole with frequency range of 2.38 to 3.01 GHz, 2.47 to 3.08 GHz and 2.53 to 3.00 GHz, respectively. Good agreement is obtained between simulated and measured results.

INDEX TERMS Evanescent-mode cavity, quadrature coupler, rat-race coupler, reconfigurable filters.

I. INTRODUCTION

Quadrature coupler and rat-race coupler are essential components and have been widely used in microwave circuits and systems [1]–[4]. Many techniques have been proposed to realize miniaturized couplers. For instances, in [5]–[7], folded microstrip lines were used to obtain compact couplers; in [8], co-planar waveguide structure was used to design coupler with broadband performance and compact size; in [9], laterally offset dual ring structure was used to realize quad-band couplers. As the demand for multi-band applications increases, reconfigurable couplers with controllable center frequency, bandwidth and power-division ratio were also proposed [10]–[13]. In [14] and [15], couplers with continuously frequency tuning have been proposed, good tuning performance was obtained, however, all of them can afford only one coupler. In [16], rat-race or branch-line coupler was demonstrated in one single unit by electrically switching, however, the capability of frequency agility is not provided.

The associate editor coordinating the review of this manuscript and approving it for publication was Feng Lin.

On the other hand, filters are also important components in microwave circuit and systems. To reduce system component counts, a great number of studies have been made to integrate coupler and filter together. In [17]–[24], different techniques have been proposed to realize the filtering couplers, however, these works only afford fixed band applications. In [25] and [26], reconfigurable filtering couplers were proposed. Even though flexible frequency tunability in these filtering couplers was achieved by controlling tunable corresponding varactors, these designs only have a simple function as either a filtering quadrature coupler or a filtering rat-race coupler, and did not allow filtering rat-race coupler and filtering quadrature coupler integrated in one single unit. In [27], a reconfigurable filter with rat-race coupler and quadrature coupler functions has been proposed, good performance has been obtained. However, the design in [27] is based on conventional microstrip line technology which has limitations of low quality factor, low power handling capability, and relatively narrow frequency tuning range.

In this paper, a novel reconfigurable multi-functional filtering coupler is proposed. It is constructed by four

substrate integrated waveguide (SIW) evanescent-mode cavity resonators. By loading piezoelectric actuators on top of each resonator and inserting varactors between adjacent resonators, the structure can achieve multiple reconfigurable functions among filtering rat-race coupler, filtering quadrature coupler, single-ended two-pole, three-pole, and four-pole filters, in addition to continuously frequency, independent bandwidth, and power-division tuning. Throughout analysis is given to demonstrate the proposed technology. Good agreement between simulation and measurement has been obtained. As compared to the work in [27], this proposed design is an independent work that has demonstrated reconfigurable multifunction filter with good performance using EVA resonator technology. By using the EVA resonator technology, it could bring advantages of low insertion loss and high power handling.

II. DESIGN

Fig. 1(a) shows the 3-D view of the proposed multi-functional four-port coupler. It is fabricated using conventional single-layer printed-circuit and consists of four (evanescent-mode) EVA cavity resonators. Each EVA cavity resonator is constructed by an inner capacitive post and a circular outer via-wall. The inner capacitive post is composed of a circular path in the middle plane which is connected to bottom plane by six metallic vias. Above the circular path, a small cavity is fabricated and piezoelectric disk actuators are placed on top of the cavity for frequency tuning [28]. The adjacent evanescent mode cavities are connected by tunable varactors placing on the bottom plane, as shown in Fig. 1(b). The input/output coupling at each port is realized by opening an arc-slot which is underneath each EVA cavity on the bottom metallic plane.

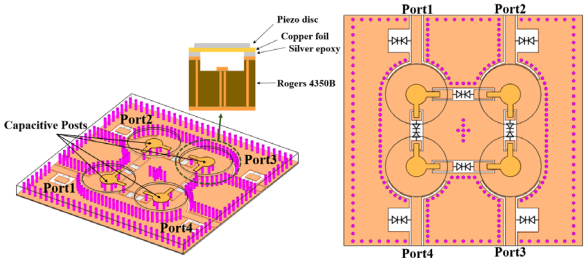

FIGURE 1. Structure of the proposed multifunction filtering coupler. (a) 3D-view. (b) Top view.

Fig. 2(a) shows the schematic of the proposed multi-functional coupler. Each evanescent-mode cavity is represented by a shunt *L*-*C* resonant tank, and the coupling between adjacent cavities *i* and *j* are represented by ideal J-invertors J_{ij}. The external coupling at the four ports is represented by J-inverters J_e.

It is well known that an ideal J-inverter can be implemented using one quarter-wave or three quarter-wave transmission line [29]. Thus, for analysis convenience, J-inverters with $-90°$ phase shift are replaced by quarter-wavelength lines, while the J-inverters with 90° phase shift are represented by three quarters-wavelength lines, as shown in fig. 2(b).

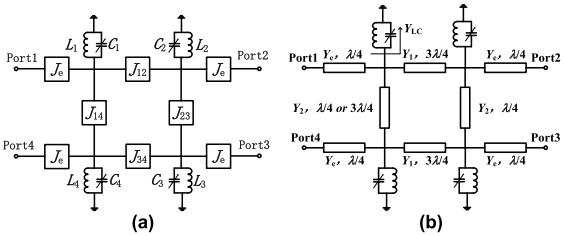

FIGURE 2. (a) Schematic of the proposed filtering coupler. (b) Equivalent circuit of the proposed filtering coupler.

The proposed four-port coupler structure can work under different function modes by reconfiguring the coupling coefficients between adjacent resonators. These function modes include the filtering quadrature coupler mode, filtering rat-race coupler mode and the multi-pole bandpass filtering mode, which will be discussed below in details.

A. FILTERING QUADRATURE COUPLER MODE

In filtering quadrature coupler mode, the coupling coefficients between adjacent resonators are configured as that J_{12} and J_{34} have 90° phase delay and J_{23} and J_{14} have -90° phase delay. Thus, the equivalent circuit in Fig. 2 can be represented by the circuit given in Fig. 3(a) where the J-inverters with $-90°$ phase shift are replaced by a quarter-wavelength lines and the J-inverters with 90° phase shift are represented by three quarters-wavelength lines. The equivalent relation between J-inverters and the characteristic admittance of the transmission lines are given as,

$$J_{12} = J_{34} = +Y_1, \quad J_{23} = J_{14} = -Y_2 \tag{1}$$

where Y_1 and Y_2 are normalized with respect to 50 Ω source impedance ($Y_1 > 0, Y_2 > 0$), the "+" sign denotes the 90° J-invertor, and the "−" sign denotes $-90°$ J-inverter. Since the structure is symmetrical with to *X*-*X'* plane, the proposed coupler can be analyzed with the even- and odd-mode analysis method, as shown in Fig. 3(b) and (c). Under even-mode excitation, a virtual open is assigned along the symmetrical plane, thus, the transmission matrix ($[ABCD]_e$) of the even mode half circuit in Fig. 3 (b) can be calculated as,

$$\begin{aligned}[ABCD]_e &= \begin{bmatrix} 1 & 0 \\ jY_2 + Y_{LC} & 1 \end{bmatrix} \begin{bmatrix} 0 & -j/Y_1 \\ -jY_1 & 0 \end{bmatrix} \begin{bmatrix} 1 & 0 \\ jY_2 + Y_{LC} & 1 \end{bmatrix} \\ &= \begin{bmatrix} (Y_2 - jY_{LC})/Y_1 & -j/Y_1 \\ -j\left(Y_1 - (Y_2 - jY_{LC})^2/Y_1\right) & (Y_2 - jY_{LC})/Y_1 \end{bmatrix} \end{aligned} \tag{2}$$

where Y_{LC} is the input admittance of the *LC* resonant tank. Similarly, under odd-mode excitation, the transmission matrix ($[ABCD]_o$) of the odd mode half circuit in Fig. 3 (c)

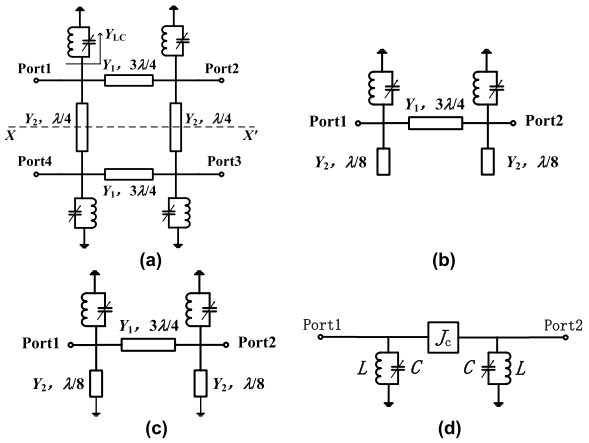

FIGURE 3. (a) Schematic of the proposed structure in filtering branch-line coupler mode. (b) Even mode half circuit. (c) Odd mode half circuit. (d) Conventional coupled resonators with J-invertor in between.

can be calculated as,

$$[ABCD]_{\mathrm{o}} = \begin{bmatrix} 1 & 0 \\ -jY_2 + Y_{\mathrm{LC}} & 1 \end{bmatrix} \begin{bmatrix} 0 & -j/Y_1 \\ -jY_1 & 0 \end{bmatrix} \begin{bmatrix} 1 & 0 \\ -jY_2 + Y_{\mathrm{LC2}} & 1 \end{bmatrix} = \begin{bmatrix} -\left(Y_2 + jY_{\mathrm{LC}}\right)/Y_1 & -j/Y_1 \\ -j\left(Y_1 - \left(Y_2 + jY_{Lc}\right)^2/Y_1\right) & -\left(Y_2 + jY_{\mathrm{LC}}\right)/Y_1 \end{bmatrix} \quad (3)$$

Assuming the working frequency is near the frequency of the resonant tank ω_0, and it has $Y_{\mathrm{LC}} \approx 0$. Converting the [ABCD] matrix in (2) and (3) to scattering matrix, the corresponding reflection and transmission coefficients under even and odd mode half circuits are obtained as,

$$\Gamma_{\mathrm{e}} = \frac{j\left(Y_1 - Y_2^2/Y_1 - 1/Y_1\right)}{2Y_2/Y_1 + j\left(Y_2^2/Y_1 - Y_1 - 1/Y_1\right)} \quad (4)$$

$$\Gamma_{\mathrm{o}} = \frac{j\left(Y_1 - Y_2^2/Y_1 - 1/Y_1\right)}{-2Y_2/Y_1 + j\left(Y_2^2/Y_1 - Y_1 - 1/Y_1\right)} \quad (5)$$

$$T_{\mathrm{e}} = \frac{2}{2Y_2/Y_1 + j\left(Y_2^2/Y_1 - Y_1 - 1/Y_1\right)} \quad (6)$$

$$T_{\mathrm{o}} = \frac{2}{-2Y_2/Y_1 + j\left(Y_2^2/Y_1 - Y_1 - 1/Y_1\right)} \quad (7)$$

Based on (4)-(7), the reflection coefficient and transmission coefficient of the four-port coupler in Fig.3 (a) can be obtained as in the following equations:

$$S_{11} = \frac{\Gamma_{\mathrm{e}} + \Gamma_{\mathrm{o}}}{2} = \frac{1/Y_1^2 - \left(Y_1 - Y_2^2/Y_1\right)^2}{(2Y_2/Y_1)^2 + \left(Y_2^2/Y_1 - Y_1 - 1/Y_1\right)^2} \quad (8)$$

$$S_{21} = \frac{T_{\mathrm{e}} + T_{\mathrm{o}}}{2} = \frac{2j(-Y_2^2/Y_1 + Y_1 + 1/Y_1)}{(2Y_2/Y_1)^2 + (Y_2^2/Y_1 - Y_1 - 1/Y_1)^2} \quad (9)$$

$$S_{31} = \frac{T_{\mathrm{e}} - T_{\mathrm{o}}}{2} = \frac{4Y_2/Y_1}{(2Y_2/Y_1)^2 + \left(Y_2^2/Y_1 - Y_1 - 1/Y_1\right)^2} \quad (10)$$

$$S_{41} = \frac{\Gamma_{\mathrm{e}} - \Gamma_{\mathrm{o}}}{2} = \frac{2(Y_2 - Y_2^3/Y_1^2 - Y_2/Y_1^2)}{(2Y_2/Y_1)^2 + (Y_2^2/Y_1 - Y_1 - 1/Y_1)^2} \quad (11)$$

Assume port 1 and 4 in the proposed quadrature coupler serve as the input and isolation port, respectively, it has,

$$S_{11} = 0 \quad (12)$$

$$S_{41} = 0 \quad (13)$$

Combing (8), (11), (12) and (13), Y_1 and Y_2 is found to have the following relation,

$$Y_1^2 = Y_2^2 + 1 \quad (14)$$

Combining (9), (10) and (14), transmission coefficient from port1 to port2 and from port1 to port3 are obtained as,

$$S_{21} = \frac{jY_1}{Y_2^2 + 1} \quad (15)$$

$$S_{31} = \frac{Y_1 Y_2}{Y_2^2 + 1} \quad (16)$$

From (15) and (16), it can be found that output port 2 and 3 have 90° phase difference, indicating an ideal quadrature coupler around the working frequency ω_0. When the frequency is away from ω_0, the input admittance of the *L-C* resonant tank increases, and provides a low-impedance path to ground, thus shorting the signal to ground and exhibiting a filtering coupler performance.

The power division ratio k_{pr} between output port 2 and 3 is found using (15) and (16) as,

$$k_{\mathrm{pr}} = \left|\frac{S_{21}^2}{S_{31}^2}\right| = \frac{1}{Y_2^2} \quad (17)$$

Combine (1), (12), (13), (15), (16) and (17), it has,

$$J_{12} = J_{34} = Y_1 = \sqrt{\frac{1 + k_{\mathrm{pr}}}{k_{\mathrm{pr}}}} \quad (18)$$

$$J_{23} = J_{14} = -Y_2 = -\sqrt{\frac{1}{k_{\mathrm{pr}}}} \quad (19)$$

Thus, it is concluded that once the power ratio between output port 2 and 3 of the quadrature coupler is specified, the value of the J-invertor between resonators can be determined to obtain a quadrature coupler with given power-division ratio.

It should be noted that equations (18) and (19) only guarantee the quadrature coupler performance with 90° phase difference and power-division ratio of k_{pr} at the outputs, they do not guarantee the desired filter performance with specific fractional bandwidth and ripple level. In order to obtain desired filter quadrature coupler performance for given filter specifications, the coupling between resonators in the proposed filter coupler needs to map with the conventional coupled resonators [26]. Fig. 3(d) shows the structure of conventional coupled resonators with J-invertor in between. Assuming the characteristic admittance of the J-invertor is J_{c}, the coupling coefficient k_{c} between the coupled resonators can be calculated from the low-pass prototype filter as,

$$J_c = FBW\frac{\omega_0 C}{\sqrt{g_1 g_2}}, \quad k_{\mathrm{c}} = \frac{J_c}{\omega_0 C} \quad (20)$$

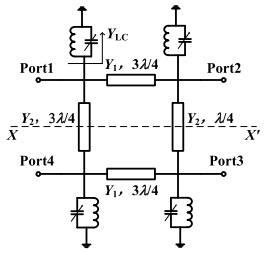

FIGURE 4. Schematic of the proposed structure in filtering rat-race coupler mode.

where FBW is the fractional bandwidth, g_1 and g_2 are element value in the corresponding low-pass prototype filter, ω_0 is the angular resonant frequency, C is the capacitance of the L-C resonant tank. The mapping of the coupling coefficients between the proposed filter coupler and the conventional coupled resonators can be approximately obtained as [30],

$$k_{12} = k_{34} = \frac{J_{12}}{\omega_0 C} \cdot J_c = \frac{J_{34}}{\omega_0 C} \cdot J_c = \sqrt{\frac{1 + k_{pr}}{k_{pr}}} k_c \tag{21}$$

$$k_{23} = k_{14} = \frac{J_{23}}{\omega_0 C} \cdot J_c = \frac{J_{14}}{\omega_0 C} \cdot J_c = -\sqrt{\frac{1}{k_{pr}}} k_c \tag{22}$$

where k_{ij} is coupling coefficient between adjacent resonators i and j in the proposed filter quadrature coupler for given filter bandwidth and ripple level. Since k_c can be calculated from the prototype filter for given filter bandwidth and ripple level [29], the k_{ij} can then obtained from (21) and (22) following the same filter requirement. The external quality factor of the proposed filter coupler stays the same with the external quality factor calculated from the coupled resonator theory for given filter requirement.

In filtering quadrature coupler mode, it is noted from (21) and (22) that the coupling coefficients k_{12} and k_{34} are positive while k_{23} and k_{14} are negative. The coupling sign depends on the physical coupling type of the coupled resonators, which usually refers to the magnetic (inductive) coupling or the electric (capacitive) coupling. If the magnetic coupling is assigned to be negative coupling, then the electric coupling will be positive coupling.

For the idea 3dB filter quadrature coupler ($k_{pr} = 1$), the required coupling coefficients between resonators are calculated as,

$$k_{12} = k_{34} = \sqrt{2} k_c, \quad k_{23} = k_{14} = -k_c \tag{23}$$

B. FILTERING RAT-RACE COUPLER MODE

In filtering rat-race coupler mode, the coupling between adjacent resonators are configured as that J_{12}, J_{14}, and J_{34} have 90° phase delay while and J_{23} have −90° phase delay. Thus, the equivalent circuit in Fig. 2 can be represented by the circuit given in Fig. 4. The J-inverters with −90° phase shift are replaced by a quarter-wavelength line while the J-inverters with 90° phase shift are represented by three quarters-wavelength line. The equivalent relation between J-inverters and transmission lines are given as,

$$J_{12} = J_{34} = J_{14} = Y_1, \quad J_{23} = -Y_2 \tag{24}$$

Port 1 and 3 are the sum and difference ports, respectively. With symmetrical plane along the X-X' plane, the proposed rat-race coupler can be analyzed using the same even- and odd-mode method as given in the previous section, and the scattering parameters of the proposed rat-race coupler can be obtained as,

$$\begin{aligned}
S_{11} &= \frac{\Gamma_{e1} + \Gamma_{o1}}{2} = \frac{1 - Y_1^2 - Y_2^2}{1 + Y_1^2 + Y_2^2} \\
S_{41} &= \frac{\Gamma_{e1} - \Gamma_{o1}}{2} = \frac{2jY_2}{1 + Y_1^2 + Y_2^2} \\
S_{21} &= \frac{T_{e1} + T_{o1}}{2} = \frac{2jY_1}{1 + Y_1^2 + Y_2^2} \\
S_{31} &= \frac{T_{e1} - T_{o1}}{2} = 0, \quad S_{13} = \frac{T_{e3} - T_{o3}}{2} = 0 \\
S_{33} &= \frac{\Gamma_{e3} + \Gamma_{o3}}{2} = \frac{1 - Y_1^2 - Y_2^2}{1 + Y_1^2 + Y_2^2} \\
S_{23} &= \frac{\Gamma_{e3} - \Gamma_{o3}}{2} = \frac{-2jY_2}{1 + Y_1^2 + Y_2^2} \\
S_{43} &= \frac{T_{e3} + T_{o3}}{2} = \frac{2jY_1}{1 + Y_1^2 + Y_2^2}
\end{aligned} \tag{25}$$

From (25), it can be seen that port 2 and 4 are 0° in phase when port 1 servers as the input, and are 180° out of phase when port 3 servers as the input. To obtain ideal match at port 1 and ideal match at port 3, it has

$$S_{11} = S_{33} = 0 \tag{26}$$

Combine (25) and (26), the relation between Y_1 and Y_2 can be obtained,

$$Y_1^2 + Y_2^2 = 1 \tag{27}$$

The power division ratio between port 2 and 4 can be calculated as,

$$k_{pr} = \left|\frac{S_{21}^2}{S_{41}^2}\right| = \left|\frac{S_{43}^2}{S_{23}^2}\right| = \frac{Y_1^2}{Y_2^2} = \frac{Y_1^2}{1 - Y_1^2} \tag{28}$$

Combine (24), (25), (26), and (28), it has,

$$J_{12} = J_{34} = J_{14} = Y_1 = \sqrt{\frac{1}{k_{pr} + 1}} \tag{29}$$

$$J_{23} = -Y_2 = -\sqrt{\frac{k_{pr}}{k_{pr} + 1}} \tag{30}$$

Thus, it is again concluded that once the power division ratio between output port 2 and 4 of the rat-race coupler is specified, the value of the J-invertor between resonators can be determined to obtain a rat-race coupler with given power-division ratio.

Similarly, in order to obtain desired filtering rat-race coupler performance for given filter specifications, the mapping of the coupling coefficients between the proposed filter rat-race coupler and the conventional coupled resonators can be approximately obtained as,

$$k_{12} = k_{34} = k_{14} = \frac{Y_1}{\omega_0 C} \cdot J_c = \sqrt{\frac{1}{k_{\rm pr}+1}} k_c \qquad (31)$$

$$k_{23} = -\frac{Y_2}{\omega_0 C} \cdot J_c = -\sqrt{\frac{k_{\rm pr}}{k_{\rm pr}+1}} k_c \qquad (32)$$

For the idea 3dB rat-race coupler ($k_{\rm pr} = 1$), the required coupling coefficients between resonators are calculated as,

$$k_{12} = k_{34} = k_{14} = \frac{1}{\sqrt{2}} k_c, \quad k_{23} = -\frac{1}{\sqrt{2}} k_c \qquad (33)$$

C. SINGLE-ENDED SECOND-ORDER/THIRD-ORDER/FOURTH-ORDER BANDPASS FILTERS MODE

In single-ended bandpass filtering mode, some ports in the coupler are left open and the coupling coefficients between adjacent resonators are reconfigured to realize second-order, third-order and fourth-order filters.

1) SECOND-ORDER BANDPASS FILTERING MODE

In this mode, port 3 and 4 are left open and coupling coefficients between resonator 1 and 2, between resonator 2 and 3, and between 3 and 4 are made to be zero as $k_{12} = k_{23} = k_{34} = 0$. Since $k_{12} = k_{23} = k_{34} = 0$, it is straightforward that the signal can only go from port 1 to port 4 through resonator 1 and resonator 4, forming a second-order bandpass filter.

2) THIRD-ORDER BANDPASS FILTERING MODE

In this mode, port 2 and 4 are left open and coupling coefficients between resonator 1 and 2, between resonator 2 and 3, are made to be zero as $k_{12} = k_{23} = 0$. Thus, the signal can only go from port 1 to port 3 through resonator 1, resonator 4 and resonator 3 in sequence, forming a third-order bandpass filter.

3) FOURTH-ORDER FILTERING MODE

In this mode, port 3 and 4 are left open and coupling coefficients between resonator 1 and 2 is made to be zero as $k_{12} = 0$. Thus, the signal can only go from port 1 to port 2 through resonator 1, 4, 3 and 2 in sequence, forming a fourth-order bandpass filter.

In Summary, the proposed four resonators structure can work under different function modes by reconfiguring the coupling coefficients between adjacent resonators.

D. ANALYSIS OF COUPLING COEFFICIENT

Fig. 5(a) and (b) shows the proposed coupling structure between the adjacent resonators. The coupling consists of an open window with a width of w between adjacent resonators and a coupling capacitor C_c connected between two

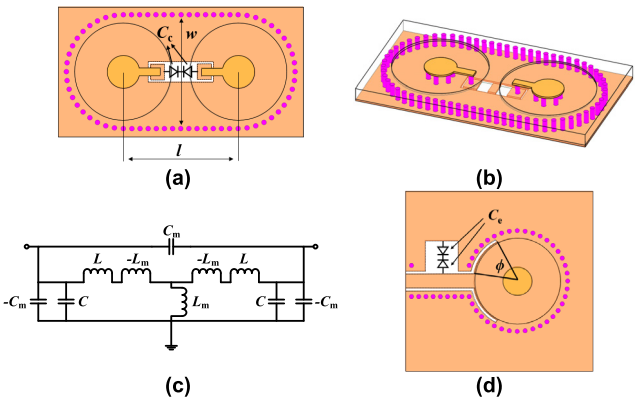

FIGURE 5. (a) The coupling structure of top-view. (b) The coupling structure of 3D-view. (c) Equivalent circuit of the coupling structure. (d) Structure of the input/output coupling.

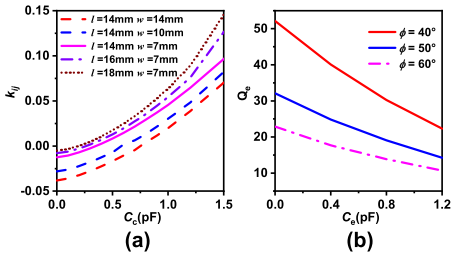

FIGURE 6. (a) k_{ij} versus C_c at different l and different w. (b) Q_e versus C_e at different ϕ.

adjacent posts. Both electric and magnetic coupling exist in the proposed coupling structure. The coupling through the open window is mainly dominated by magnetic coupling in nature [30] while the coupling from the coupling capacitator C_c mainly contributed to the electric coupling [31]. Fig. 5 (c) shows equivalent mixed coupling circuit of the proposed structure. An impedance inverter $K = \omega L_m$ and an admittance inverter $J = \omega C_m$ was used to represent the magnetic coupling and the electric coupling, respectively [29]. The coupling coefficient k_{ij} is mixed coupling of magnetic coupling k_m and electric coupling k_e as [29],

$$k_{ij} = \frac{C_m}{C} - \frac{L_m}{L} = k_e - k_m \qquad (34)$$

When the magnetic coupling k_m is larger than the electric coupling k_e, the total coupling k_{ij} is dominated by the magnetic coupling and verse vice. The magnetic coupling k_m can be controlled by the width window w and distance l between two adjacent resonators while the electric coupling k_e can be controlled by the value of the coupling capacitance.

Fig. 6(a) shows the extracted coupling coefficients versus coupling capacitance at different width w and distance l using the method given in [29]. As can be observed, the coupling k_{ij} can be tuned from a negative value to zero and from zero to positive. When the coupling capacitance is week, the coupling is mainly dominated the magnetic coupling in nature ($k_e < k_m$); When the coupling capacitance increases, the electrical coupling between adjacent resonators increases.

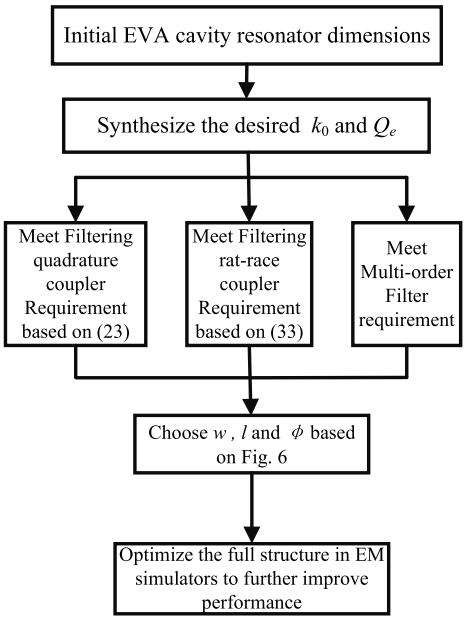

FIGURE 7. Design process for the proposed filtering coupler.

When it reaches a certain value C_t, the electric coupling cancels out the magnetic coupling ($k_e = k_m$), resulting in zero coupling. As the coupling capacitance increases from C_t, the electrical coupling keeps increasing and becomes larger than the magnetic coupling. The total coupling is dominated by electric coupling ($k_e > k_m$).

Therefore, by using the proposed the coupling structure, the coupling coefficients between adjacent resonators can be easily controlled to be either magnetic coupling or electric coupling or zero, so as to satisfy the requirements for filtering rat-race coupler mode, filtering quadrature coupler mode, and single- ended filtering mode. The required inter-stage coupling between adjacent resonators under different filter modes can be approximated read from Fig. 6(a).

The input/output coupling of the four ports is determined by size of the opening slots on the top plane, as shown in Fig. 5(d). To introduce more tuning flexibility, a shunt capacitance to ground is added at the input/output lines. Fig. 6(b) shows the extracted external coupling versus the shunt capacitance value. As can be observed, the Q_e values can be controlled by changing the opening angle size of the slot ϕ and varactor C_e. The required input/output coupling for different filtering modes can be approximated read from Fig. 6(b). A flowchart of this process is shown in Fig. 7.

III. SIMULATIONS AND MEASUREMENTS

The filtering crossover is designed to have quasi-Chebyshev response with a 3-dB FBW of 5% with ripple level of 0.1 dB, and the center frequency of 2.64 GHz is designed for the filtering coupler. The design parameters corresponding to these specifications can be obtained in Fig. 6 and Table 1.

The proposed reconfigurable multifunctional filter was fabricated on Rogers 4350B with dielectric constant $\varepsilon_r = 3.66$ and thickness $h = 1.524$ mm. A post radius of 2mm is chosen, which corresponds to two 2.56-mm branches. Commercial piezoelectric disk actuators with a diameter of 12.7-mm and thickness of 0.38 mm are used. The actuator can provide up to 40-um of free–free displacement. The inter-resonator and external coupling control network is on the backside of the substrate as shown in Fig. 1(b). GaAs varactors MA46H201 ($C_j = 0.3 \sim 23$ pF) from Macom Inc. were used to control the inter-stage coupling and external coupling control, respectively. The photograph of the fabricated filter are shown in Fig. 8 and it occupies a footprint size of $0.31\lambda_g \times 0.32\lambda_g$, where λ_g is the guided wavelength at the lowest frequency (2.08 GHz).

TABLE 1. Physical dimensions.

w	l	ϕ
7mm	14mm	50°

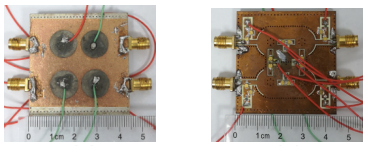

FIGURE 8. Photograph of the fabricated multifunctional filter. (a) Top view. (b) Bottom view.

A. SIMULATED AND MEASURED RESULTS OF QUADRATURE FILTERING COUPLER

In filtering quadrature coupler mode, the coupling between resonators is tuned to satisfy the equation (21) and (22) by controlling the coupling varactors. Fig. 9 presents the measured and simulated S_{21} and S_{31} of the proposed quadrature filtering coupler with $k_{pr} = 1$. Measurement agrees well with the simulation. The center frequency of the filtering coupler can be tuned from 2.08 to 3.00 GHz with insertion loss from 2.68 to 3.30 dB. The amplitude imbalance between S_{21} and S_{31} is less than 0.3 dB across the passband. The measured return loss at port 1 and isolation at port 4. The measured reflection and isolation are better than 10.22 and 15.13 dB, respectively, for all tuning states. The measured phase imblance is less than 5° within 30MHz bandwidth.

By controlling the coupling amount between the resonators, the power-division ratio k_{pr} between port 2 and 3 can be also adjusted. Fig. 10 presents the measured and simulated S-parameters under different power-division ratios of 1 dB, 3 dB and 5 dB in filtering quadrature coupler mode. The measures insertion losses (S_{21} and S_{31}) for the cases of 1dB, 3dB and 5dB power-division ratios at 2.64 GHz are (5.56dB and 6.49dB), (4.46dB and 7.46dB) and (3.58dB and 8.54dB), respectively. Note that the ideal insert loss in lossless case for the cases of 1dB, 3dB and 5dB power-division ratios are (3.53 and 2.53 dB), (4.77 and 1.77 dB), and (6.19 and 1.19 dB). The measured phase imbalance is

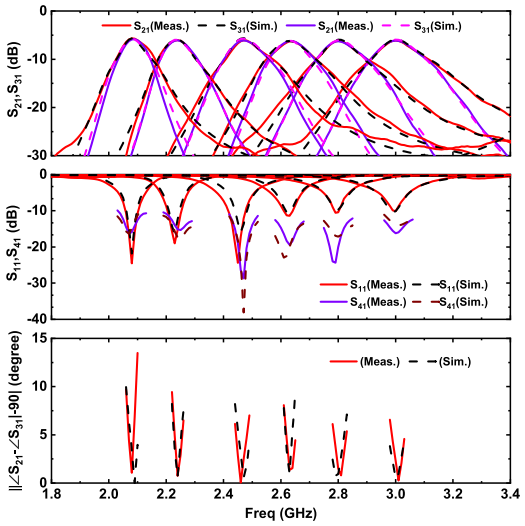

FIGURE 9. Measured and simulated results of the proposed idea 3dB filtering quadrature hybrid coupler.

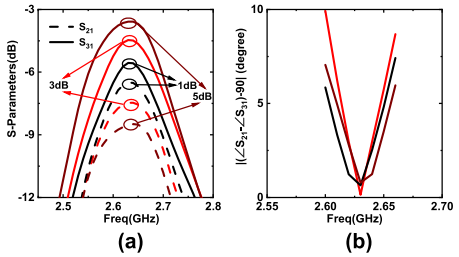

FIGURE 10. Measured different power-dividing ratio in filtering quadrature hybrid coupler mode. (a) S-parameters. (b) Phase imbalance.

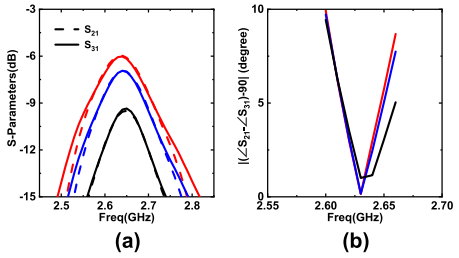

FIGURE 11. Measured bandwidth control in filtering quadrature hybrid coupler mode (with $k_{pr} = 1$). (a) S-parameters. (b) Phase imbalance.

less than 5° within 40MHz bandwidth under different power-division ratios.

Fig. 11 presents the measured and simulated S-parameters of proposed quadrature filtering coupler for bandwidth control. The 1-dB bandwidth can vary in the range of 60 - 75 MHz. The measured insertion loss decreases with the increasing bandwidth. The phase imbalance is less than 5° within 30MHz bandwidth.

B. SIMULATED AND MEASURED RESULTS OF RAT-RACE FILTERING COUPLER

In filtering rat-race coupling mode, the coupling between resonators is reconfigured to satisfy the equation (28) and (32). Fig. 12 shows the measured and simulated S-parameters

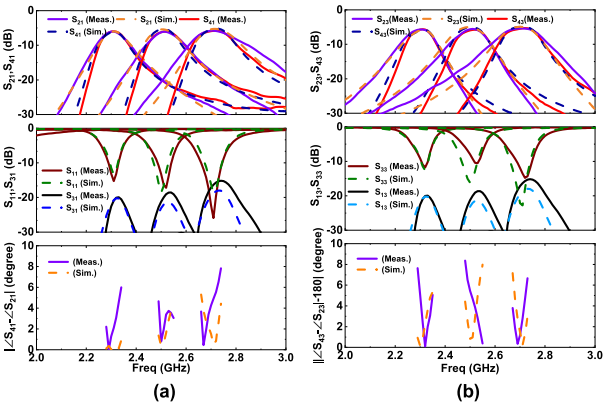

FIGURE 12. Measured and simulated S-parameters of the proposed filtering rat-race coupler. (a) excited from port 1. (b) excited from port 3.

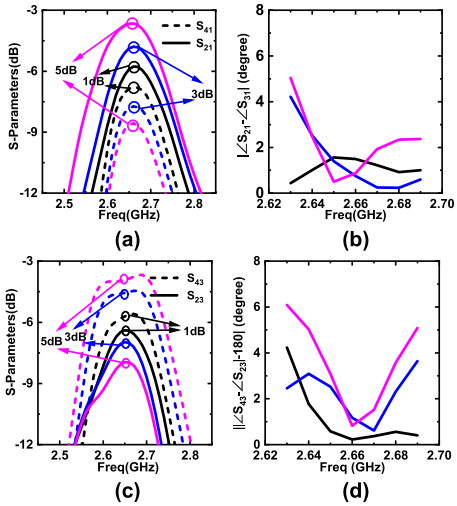

FIGURE 13. Measured different power-division ratio in filtering rat-race coupler mode. (a) S-parameters excited from port 1. (b) Phase imbalance excited from port 1. (c) S-parameters excited from port 3. (d) Phase imbalance excited from port 3.

in filtering rat-race coupling mode with $k_{pr} = 1$ (0 dB). When excited from port 1 (sum port), it has an equal power dividing and 0° phase difference between ports 2 and 4, and the passband can be tuned from 2.31 to 2.71 GHz. The measured insertion loss of S_{21} and S_{41} varies from 2.84 to 3.1 dB within the full tuning range. The reflection at port 1 and isolation at port 3 is better than 15.29 and 17.19 dB, respectively. The measured phase imbalance and amplitude imbalance between S_{21} and S_{41} are better than 8° and 0.4 dB, respectively. When excited from port 3 (differential port), it has an equal power dividing and 180° phase difference between ports 2 and 4; the passband can be also tuned from 2.31 to 2.71 GHz. The measured insertion loss of S_{23} and S_{43} varies from 2.36 to 3.79 dB within the full tuning range. The reflection at port 3 and isolation at port 1 is better than 10.42 and 16.32dB. The measured phase imbalance and amplitude imbalance between S_{21} and S_{41} are better than 8.5° and 0.4 dB, respectively.

Fig. 13 presents the measured and simulated S-parameters in filtering rat-race coupling mode with $k_{pr} = 1$ dB, 3 dB and 5 dB at 2.65 GHz. When excited from port 1 (sum port),

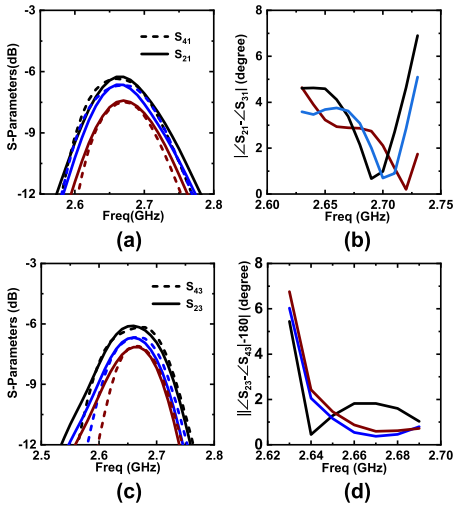

FIGURE 14. Measured bandwidth control in filtering rat-race coupler mode. (a) S-parameters excited from port 1. (b) Phase imbalance excited from port 1. (c) S-parameters excited from port 3. (d) Phase imbalance excited from port 3.

the measured insertion loss of (S_{21} and S_{41}) for $k_{\rm pr} = 1$, 3 and 5 dB are (6.79 and 5.77 dB), (7.73 and 4.794 dB), and (8.567 and 3.65 dB), respectively. Note that the ideal insert loss in lossless case of (S_{21} and S_{41}) for $k_{\rm pr} = 1$, 3 and 5 dB are (3.53 and 2.53 dB), (4.77 and 1.77 dB), and (6.19 and 1.19 dB), respectively. Thus, the average insertion loss for S_{21} and S_{41} is less than 2.8 dB. The phase imbalance for S_{21} and S_{41} is again less than 5° within 50MHz bandwidth. When excited from port 3 (differential port), the measured insertion loss of (S_{23} and S_{43}) for $k_{\rm pr} = 1$, 3 and 5 dB are (6.42 and 5.62 dB), (7.01 and 4.50 dB), and (7.97 and 3.85dB), respectively, with a maximum phase error of ±5° within 50MHz bandwidth. The average insertion loss for S_{23} and S_{43} is less than 3 dB. The phase imbalance for S_{23} and S_{43} is again less than 5° within 50MHz bandwidth.

Fig. 14 presents the measured and simulated S-parameters of proposed rat-race filtering coupler for bandwidth control. As can be observed, the −1 dB bandwidth for the passband can be tuned from 70 to 90 MHz, while keeping good phase and amplitude imbalance.

C. SIMULATED AND MEASURED RESULTS OF SECOND-ORDER, THIRD-ORDER AND FOURTH-ORDER FILTERS

In second-order bandpass filtering mode, port 3 and 4 are left open and coupling coefficients between resonator 1 and 2, between resonator 2 and 3, and between 3 and 4 are made to be zero as $k_{12} = k_{23} = k_{34} = 0$. Fig. 15 (a) presents the measured and simulated S-parameters in second-order bandpass filtering mode between port 1 and 2. Good agreement is observed between simulation and measurement. The center frequency can be tuned from 2.38 to 3.01 GHz with insertion loss varying from 1.1 to 2.64 dB and constant absolute-bandwidth of 25-MHz. The stopband suppression at frequency of 100MHz away from center frequency is about 10 dB.

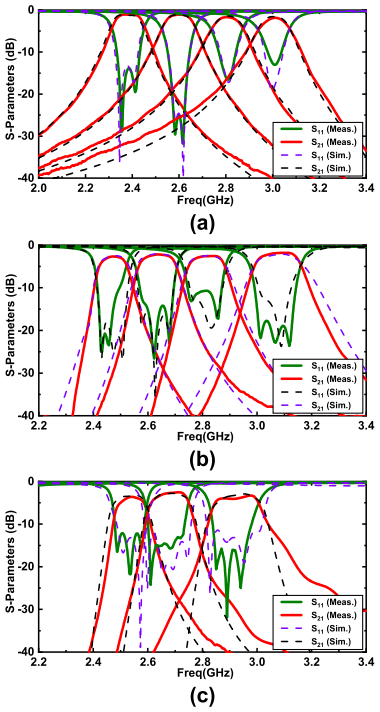

FIGURE 15. Measured S parameters for multiple-order. (a) second-order filters. (b) third-order filters. (c) fourth-order filters.

By floating port 2 and 4 and making coupling coefficients $k_{12} = k_{23} = 0$, the proposed coupler can work as a conventional third-order bandpass filter between port 1 and 3. Fig. 15 (b) presents the measured and simulated S-parameters in third-order bandpass filtering mode. Again, good agreement is observed between simulation and measurement. The center frequency can be tuned from 2.47 to 3.08 GHz with insertion loss varying from 1.79 to 2.67 dB. The stop band suppression at frequency of 100MHz away from center frequency is about 20 dB.

Similarly, when port 3 and 4 are left open and coupling coefficients between resonator 1 and 2 are made to be zero as $k_{12} = 0$, the proposed coupler can work as a conventional fourth-order bandpass filter between port 1 and 2. Fig. 15 (c) presents the measured and simulated S-parameters in fourth-order bandpass filtering mode. The center frequency can be tuned from 2.53 to 3 GHz. The measured insertion loss varys from 3.2 to 3.6 dB. The stopband suppression at frequency of 100MHz away from center frequency is better than 30 dB. Note than the tuning range for the four-order bandpass filter is narrower than the third- and second-order counterparts, this is because more varactors are involved in the tuning process for four-order bandpass filter than for the third- and second-order counterparts, and some varactors may have smaller tuning ranges than others, thus, limiting the full tuning range for the fourth-order bandpass filter.

Table 2 gives the comparison between this proposed work and other state-of-the-art reconfigurable filtering couplers. The proposed reconfigurable filtering coupler has

TABLE 2. Comparison with other filtering couplers.

Ref.	Filtering Mode	Tech	Freq. (GHz)	IL (dB)	Size ($\lambda g \times \lambda g$)	1-dB BW Tuning	power-dividing-ratio
[29]	Quadrature hybrid coupler	Varactor	0.947-1.775	4.6±0.7/6.7±1.6	0.23×0.23	Yes	No
[29]	Rat-race filtering coupler	Varactor	0.7-1.84	4.5±0.6/4.1±1.2	0.19×0.18	Yes	No
[30]	Rat-race filtering coupler	Piezo(EVA)	0.885-1.65	1.6 ± 0.4	0.14×0.14	No	No
[27]	Quadrature hybrid coupler	Microstripe line and Varactor	1.21~1.67	3.2 ± 0.5	0.1×0.7	Yes	Yes
	Rat-race coupler		1.2~1.61	3.1 ± 0.7		Yes	Yes
	Second-order filter		1.12~1.6	2.55 ± 0.55		-	-
	Third-order filter		1.16~1.6	2.95 ± 0.65		-	-
	Fourth-order filter		1.2~1.61	3.4 ± 0.6		-	-
This work	Quadrature hybrid coupler	Piezo(EVA) and Varactor	2.08-3.00	2.99 ± 0.31	0.31×0.32	Yes	Yes
	Rat-race coupler		2.31-2.71	2.97 ± 0.13		Yes	Yes
	Second-order filter		2.38-3.01	1.87 ± 0.77		-	-
	Third-order filter		2.47-3.08	2.23 ± 0.44		-	-
	Fourth-order filter		2.53-3.0	3.4 ± 0.2		-	-

successfully realized three reconfigurable functions in one single unit using the EVA resonator technology. As compared to the work in [27], this proposed work exhibits lower insertion loss due to the higher quality factor in EVA resonators. It should be noted that the insertion loss of this proposed work is still limited by the varactors loaded between resonators. The insertion loss may be significantly improved by replacing the current varactors with MEMS varactors, and is expected be much better than that of the work in [27] with the same MEMS varactors. Meanwhile, the power handling is also expected to be better than the work in [27].

IV. CONCLUSION

A novel reconfigurable filtering coupler utilizing EVA resonators is presented. It can achieve rat-race filtering coupler, quadrature filtering coupler and multiple-order filters with frequency, bandwidth and power-dividing ratio controls, demonstrating excellent tuning capabilities. Good agreement between the measured and simulated results has been obtained.

REFERENCES

[1] W. M. Dyab, A. A. Sakr, and K. Wu, "Dually-polarized butler matrix for base stations with polarization diversity," *IEEE Trans. Microw. Theory Techn.*, vol. 66, no. 12, pp. 5543–5553, Dec. 2018.

[2] P.-L. Chi, "Miniaturized ring coupler with arbitrary power divisions based on the composite right/left-handed transmission lines," *IEEE Microw. Wireless Compon. Lett.*, vol. 22, no. 4, pp. 170–172, Apr. 2012.

[3] H.-R. Ahn and M. M. Tentzeris, "Compact and wideband general coupled-line ring hybrids (GCRHs) for arbitrary circumferences and arbitrary power-division ratios," *IEEE Access*, vol. 7, pp. 33414–33423, 2019.

[4] P.-L. Chi and T. Itoh, "Miniaturized dual-band directional couplers using composite right/left-handed transmission structures and their applications in beam pattern diversity systems," *IEEE Trans. Microw. Theory Techn.*, vol. 57, no. 5, pp. 1207–1215, May 2009.

[5] H. Ghali and T. A. Moselhy, "Miniaturized fractal rat-race, branch-line, and coupled-line hybrids," *IEEE Trans. Microw. Theory Techn.*, vol. 52, no. 11, pp. 2513–2520, Nov. 2004.

[6] R. K. Settaluri, A. Weisshaar, C. Lim, and V. K. Tripathi, "Design of compact multilevel folded-line RF couplers," *IEEE Trans. Microw. Theory Techn.*, vol. 47, no. 12, pp. 2331–2339, 1999.

[7] M. Caillet, M. Clenet, A. Sharaiha, and Y. M. M. Antar, "A compact wide-band rat-race hybrid using microstrip lines," *IEEE Microw. Wireless Compon. Lett.*, vol. 19, no. 4, pp. 191–193, Apr. 2009.

[8] T. T. Mo, Q. Xue, and C. H. Chan, "A broadband compact microstrip rat-race hybrid using a novel CPW inverter," *IEEE Trans. Microw. Theory Techn.*, vol. 55, no. 1, pp. 161–167, Jan. 2007.

[9] S. Velan, S. Kingsly, M. Kanagasabai, M. G. N. Alsath, Y. P. Selvam, and S. Subbaraj, "Quad-band rat-race coupler with suppression of spurious pass-bands," *IEEE Microw. Wireless Compon. Lett.*, vol. 26, no. 7, pp. 490–492, Jul. 2016.

[10] K.-K.-M. Cheng and M.-C.-J. Chik, "A frequency-compensated rat-race coupler with wide bandwidth and tunable power dividing ratio," *IEEE Trans. Microw. Theory Techn.*, vol. 61, no. 8, pp. 2841–2847, Aug. 2013.

[11] P.-L. Chi and T.-C. Hsu, "Highly reconfigurable quadrature coupler with ideal impedance matching and port isolation," *IEEE Trans. Microw. Theory Techn.*, vol. 65, no. 8, pp. 2930–2941, Aug. 2017.

[12] F. Lin, "A planar balanced quadrature coupler with tunable power-dividing ratio," *IEEE Trans. Ind. Electron.*, vol. 65, no. 8, pp. 6515–6526, Aug. 2018.

[13] K.-K.-M. Cheng and S. Yeung, "A novel rat-race coupler with tunable power dividing ratio, ideal port isolation, and return loss performance," *IEEE Trans. Microw. Theory Techn.*, vol. 61, no. 1, pp. 55–60, Jan. 2013.

[14] F. Lin, Q.-X. Chu, and Z. Lin, "A novel tri-band branch-line coupler with three controllable operating frequencies," *IEEE Microw. Wireless Compon. Lett.*, vol. 20, no. 12, pp. 666–668, Dec. 2010.

[15] P.-L. Chi, H.-M. Lin, and C.-P. Chien, "A tunable balanced coupler with improved phase balance and extended bandwidth," *IEEE Access*, vol. 7, pp. 37927–37935, 2019.

[16] H. N. Chu, H.-C. Liao, G.-Y. Li, and T.-G. Ma, "Novel phase reconfigurable synthesized transmission line and its application to reconfigurable hybrid coupler," in *Proc. 12th Eur. Microw. Integr. Circuits Conf. (EuMIC)*, Nuremberg, Germany, Oct. 2017, pp. 1077–1080.

[17] C.-K. Lin and S.-J. Chung, "A Compact Filtering 180° Hybrid," *IEEE Trans. Microw. Theory Techn.*, vol. 59, no. 12, pp. 3030–3036, Dec. 2011.

[18] C.-F. Chen, T.-Y. Huang, C.-C. Chen, W.-R. Liu, T.-M. Shen, and R.-B. Wu, "A compact filtering rat-race coupler using dual-mode stub-loaded resonators," in *IEEE MTT-S Int. Microw. Symp. Dig.*, Jun. 2012, pp. 1–3.

[19] L.-S. Wu, B. Xia, W.-Y. Yin, and J. Mao, "Collaborative design of a new dual-bandpass 180° hybrid coupler," *IEEE Trans. Microw. Theory Techn.*, vol. 61, no. 3, pp. 1053–1066, Mar. 2013.

[20] H. Uchida, N. Yoneda, Y. Konishi, and S. Makino, "Bandpass directional couplers with electromagnetically-coupled resonators," in *IEEE MTT-S Int. Microw. Symp. Dig.*, San Francisco, CA, USA, Jun. 2006, pp. 1563–1566.
[21] K. Wang, X. Y. Zhang, S. Y. Zheng, and Q. Xue, "Compact filtering rat-race hybrid with wide stopband," *IEEE Trans. Microw. Theory Techn.*, vol. 63, no. 8, pp. 2550–2560, Aug. 2015.
[22] T.-W. Lin, J.-Y. Wu, and J.-T. Kuo, "Filtering rat-race coupler with transmission zeros using compact miniaturized hairpin resonators," in *Proc. IEEE Int. Wireless Symp. (IWS 2015)*, Shenzhen, China, Mar. 2015, pp. 1–4.
[23] W.-H. Wang, T.-M. Shen, T.-Y. Huang, and R.-B. Wu, "Miniaturized rat-race coupler with bandpass response and good stopband rejection," in *IEEE MTT-S Int. Microw. Symp. Dig.*, Boston, MA, USA, Jun. 2009, pp. 709–712.
[24] J.-X. Xu, X. Y. Zhang, and H.-Y. Li, "Compact narrowband filtering rat-race coupler using quad-mode dielectric resonator," *IEEE Trans. Microw. Theory Techn.*, vol. 66, no. 9, pp. 4029–4039, Sep. 2018.
[25] F. Lin and H. Ma, "Design of a class of filtering couplers with reconfigurable frequency," *IEEE Trans. Microw. Theory Techn.*, vol. 66, no. 9, pp. 4017–4028, Sep. 2018.
[26] M. F. Hagag, M. Abu Khater, M. D. Sinanis, and D. Peroulis, "Ultra-compact tunable filtering rat-race coupler based on half-mode SIW evanescent-mode cavity resonators," *IEEE Trans. Microw. Theory Techn.*, vol. 66, no. 12, pp. 5563–5572, Dec. 2018.
[27] X. Zhu, T. Yang, P.-L. Chi, and R. Xu, "Novel reconfigurable filtering rat-race coupler, branch-line coupler, and multiorder bandpass filter with frequency, bandwidth, and power division ratio control," *IEEE Trans. Microw. Theory Techn.*, early access, doi: 10.1109/TMTT.2019.2959769.
[28] S. Moon, H. H. Sigmarsson, H. Joshi, and W. J. Chappell, "Substrate integrated evanescent-mode cavity filter with a 3.5 to 1 tuning ratio," *IEEE Microw. Wireless Compon. Lett.*, vol. 20, no. 8, pp. 450–452, Aug. 2010.
[29] J.-S. Hong and M. J. Lancaster, *Microstrip Filters for RF/Microwave Applications*, vol. 167. Hoboken, NJ, USA: Wiley, 2004.
[30] Q. Liu, D. Zhou, D. Zhang, and D. Lv, "A novel frequency-dependent coupling with flexibly controllable slope and its applications on substrate-integrated waveguide filters," *IEEE Microw. Wireless Compon. Lett.*, vol. 28, no. 11, pp. 993–995, Nov. 2018.
[31] X. Zhu, T. Yang, P.-L. Chi, and R. Xu, "Novel reconfigurable single-to-balanced, power-dividing, and single-ended filter with frequency and bandwidth control," *IEEE Trans. Microw. Theory Techn.*, vol. 67, no. 2, pp. 670–682, Feb. 2019.

JUNCHEN LAI was born in Yibin, Sichuan, China. He is currently pursuing the Ph.D. degree in electromagnetic field and microwave technology with the University of Electronic Science and Technology of China, Chengdu, China. His current research interests include millimeter wave circuit theory and technology, passive microwave, and millimeter-wave components.

TAO YANG (Senior Member, IEEE) received the B.Eng. and Ph.D. degrees from the University of Electronic Science and Technology of China (UESTC), Chengdu, China, in 2005 and 2011, respectively.

From February 2016 to September 2017, he was a R&D IC Engineer with Broadcom Ltd., San Jose, CA, USA. From April 2014 to February 2016, he was with Qualcomm Inc., San Diego, CA. From October 2012 to April 2014, he was with the Department of Electrical and Computer Engineering, University of California at San Diego (UCSD). From August 2011 to September 2012, he was with the Institut d'Electronique et de Telecommunications de Rennes (IETR) and the Université de Rennes 1, Rennes, France. From September 2008 to September 2010, he was a Visiting Scholar with the Electrical Engineering Department, University of California at Los Angeles (UCLA). He is currently a Professor with the University of Electronic Science and Technology of China. His research interest includes Ka-band circuit designs, such as Ka-band frequency synthesizers and transceivers, miniaturized passive microwave and millimeter-wave components, such as filters, diplexers, triplexers, and baluns, broadband microstrip antennas and leaky-wave antennas, metamaterial-based microwave circuits, design and development of RF passive components for highly integrated RF integrated circuits in deep sub-micrometer CMOS and silicon-on-insulator (SOI) technologies, and development of high Q FBAR resonators and filters.

PEI-LING CHI (Senior Member, IEEE) received the B.S. and M.S. degrees in communication engineering from National Chiao Tung University (NCTU), Hsinchu, Taiwan, in 2004 and 2006, respectively, and the Ph.D. degree in electrical engineering from the University of California at Los Angeles (UCLA), in 2011.

Since 2011, she has been with National Chiao Tung University, as an Assistant Professor of electrical and computer engineering, where she is currently an Associate Professor. She holds several U.S. and international patents in the area of the left-handed metamaterials. Her research interests include the analysis and design of the left-handed metamaterial circuits, design of microwave components and integrated systems, and the development of millimeter-wave/terahertz antennas and communications.

Dr. Chi was a recipient of the Research Creativity Award from the National Science Council, Taiwan, in 2004.

RUIMIN XU (Member, IEEE) was born in Leshan, Sichuan, China, in 1958. He received the B.S. and Ph.D. degrees in electromagnetic field and microwave techniques from the University of Electronic Science and Technology of China (UESTC), Chengdu, China, in 1982 and 2007, respectively.

He is currently a Full Professor with UESTC. His current research interests include microwave and millimeter-wave technologies and applications, and radar systems.